Journal of Applied Electrochemistry (2006) 36:1241–1252
DOI 10.1007/s10800-006-9183-2

Copper dissolution in the presence of a binary 2D-compound: CuI on Cu(100)

P. BROEKMANN*, N.T.M. HAI and K. WANDELT
Institut für Physikalische und Theoretische Chemie, Universität Bonn, Wegelerstr. 12, D-53115, Bonn, Germany
*(*author for correspondence, e-mail: broekman@thch.uni-bonn.de)*

Received 29 September 2005; accepted in revised form 20 April 2006

Key words: copper corrosion, passivation, binary compound formation, STM

Abstract

Exposing a Cu(100) electrode surface to an acidic and iodide containing electrolyte (5 mM H_2SO_4/1 mM KI) leads to the formation of an electro-compressible/electro-decompressible c(p × 2)-I adsorbate layer at potentials close to the onset of the copper dissolution reaction. An increase of mobile CuI monomers on-top of the iodide modified electrode surface causes the local CuI solubility product to be exceeded thereby giving rise to the nucleation and growth of a laterally well ordered 2D-CuI film at potentials below 3D-CuI_{bulk} phase formation. Step edges serve as sources for the consumption of copper material upon compound formation leading to accelerated copper dissolution at the step edges. The 2D-CuI film exhibits symmetry properties and nearest neighbor spacings that are closely related to the (111) lattice of the crystalline CuI_{bulk} phase. Intriguingly, the 2D-CuI film on Cu(100) does not act as an efficient passive layer. Copper dissolution proceeds at slightly higher potentials even in the presence of this binary 2D-compound via an inverse step flow mechanism. Further dissolution causes the nucleation and growth of 3D-CuI clusters on-top of the 2D-CuI film. This several nanometer thick 3D-CuI_{bulk} phase passivates the electrode against further dissolution. Characteristically, the formation/dissolution of the 3D-CuI_{bulk} phase reveals a significantly larger potential hysteresis of about $\Delta E = 320$ mV while the appearance/disappearance of the 2D-CuI film is reversible with a potential hysteresis of only $\Delta E = 20$ mV.

1. Introduction

Copper has attracted great attention over the last two decades due to its application as silicon chip interconnect material [1, 2], replacing the traditional vacuum deposited aluminum-based interconnects. This major change in state-of-the-art chip fabrication occurred after invention of the damascene copper electroplating process at IBM in the early 1990s [1]. The on-going trend of miniaturization towards the nanometer scale requires a more sophisticated understanding of the relevant interface properties of those devices containing such reactive materials as copper. An atomic scale understanding of copper corrosion phenomena, corrosion inhibition by organics [3–6], oxidation and precursor films for oxidation [7–10], anodic dissolution [11–17] and the formation of passive films [18, 19] is thus of vital interest and has consequently been the focus of numerous fundamental studies. Since modern processing lines of chip fabrication also include ''wet'' chemical deposition processes the mastering of copper-electrolyte interfaces with or without potential control can be regarded as a particular challenge.

Local phenomena of copper dissolution in acidic electrolytes have been intensively studied using *in situ* STM [11–16]. Active sites for dissolution or deposition are exclusively kinks at step edges. Magnussen and coworkers found that the local structure of kink sites can be significantly altered due to the presence of specifically adsorbed anions thus leading to changes in the overall surface reactivity. State-of-the-art video STM techniques nowadays allow direct correlation between integral macroscopic parameters such as the ''exchange current density'' and the local and microscopic dissolution rates at kink sites [14].

Substantial contributions to our microscopic understanding of the copper dissolution reaction in *alkaline electrolytes* came from Marcus et al. [8–10, 18, 19]. In contrast to the behavior in acidic media dissolution under alkaline conditions is affected by a binary compound formation, namely a passivating Cu_2O film at lower potentials and a Cu_2O/CuO, $Cu(OH)_2$ duplex film at higher potentials. Experimental conditions such as pH, applied potential and polarization time are decisive parameters which control atomic scale ordering, film morphology and passive layer thickness [18, 19].

In the present study we report a dissolution/corrosion mechanism which comprises characteristic elements of the dissolution mechanism observed in both acidic and alkaline electrolytes. A binary compound formation can

also be observed in acidic electrolytes, provided the solution phase contains species which form insoluble salts with cuprous Cu^+ ions.

The main focus of the present work lies in the structural characterization of a well ordered 2D-CuI film which appears at potentials below the regime of 3D-CuI_{bulk} phase formation. Further attention is paid to the structural stability of the 2D-CuI film against further dissolution.

2. Experimental

All experiments presented in this paper were carried out using a home-built electrochemical STM [20]. Tunneling tips were electrochemically etched in 2 M KOH solution from 0.25 mm tungsten wire and subsequently coated with hot glue. For all solutions high purity water (Milli-Q purification system; conductivity < 18 MΩ·cm; TOC < 5 ppb) and reagent grade chemicals were used. The electrolyte was purged with argon several hours before use. All potentials refer to a RHE reference.

Prior to each experiment the copper surface was treated by electrochemical etching for the removal of the native oxide film [20]. After etching the sample was rinsed with degassed 10 mm sulfuric acid solution and mounted in the electrochemical cell of the STM. All experiments started routinely with a characterization of the Cu(100) electrode exposed to 5 mm H_2SO_4 solution which also served as supporting electrolyte for all subsequent dissolution experiments in the presence of iodide. For these latter experiments the pure supporting electrolyte had to be exchanged without losing potential control by a mixture of 5 mm H_2SO_4 and 1 mm KI solution at $E = +50$ mV versus RHE. For all electrolyte exchange procedures we used an external electrolyte supply system in combination with a sophisticated pumping system which allowed an electrolyte exchange without opening the STM chamber and without losing the protective argon gas atmosphere [20].

3. Results

3.1. *Electrochemistry*

Representative CVs of Cu(100) in the pure and the iodide containing electrolyte are presented in Figure 1. The dotted black curve contains all major features of the CV of Cu(100) in dilute sulfuric acid solution [13], namely an extended double layer regime between -260 mV and $+260$ mV that is confined by the starting copper dissolution at the anodic limit and the hydrogen evolution reaction (HER) at the cathodic limit.

The CV of Cu(100) in the iodide containing electrolyte (black curve in Figure 1) reveals a number of deviations from that of the blank supporting electrolyte. Beginning with the cathodic limit it is obvious that the presence of iodide anions causes a significant shift of the onset

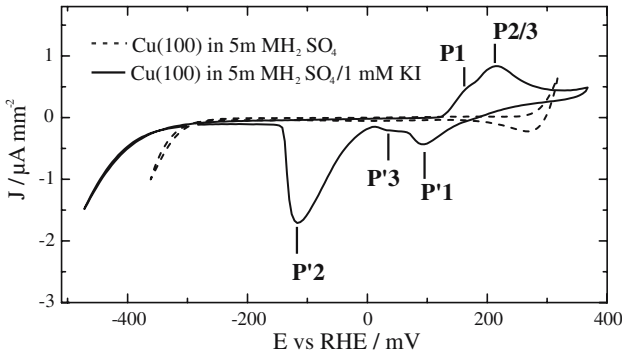

Fig. 1. (a) Cyclic voltammograms of Cu(100) in pure 5 mm H_2SO_4 and in 5 mm H_2SO_4/1 mM KI, $dE/dt = 10$ mV s^{-1}.

potential of the HER towards lower potentials ($\Delta E \approx 60$ mV). Furthermore, the exponential increase in the reduction current is much steeper in the pure sulfuric acid electrolyte than in the iodide containing solution. Both observations point to reduced reactivity of the copper electrode with respect to the HER caused by the blocking of reactive sites in the presence of adsorbed iodide. Laterally ordered iodide layers have been reported for Cu(100) at the on-set of the HER [21, 22]. The most striking deviations from the CV in the pure supporting electrolyte concern the anodic limit where a pronounced anodic peak system appears with P1 at $+175$ mV and P2/3 centered at about $+215$ mV. In the reverse scan cathodic current waves emerge at $+120$ mV (P′1), -110 mV (P′2) and $+40$ mV (P′3). The lack of an exponentially increasing anodic current within the potential range in Figure 1 indicates a surface passivation upon passing P1–P3.

In general, the overall shape of the CV of Cu(100) in the "blank" electrolyte is unaltered upon shifting the anodic potential limit. For the iodide containing electrolyte there is, however, a considerable change in the CV when the anodic potential limit is gradually shifted to higher potentials (Figure 2). CV 1 and 2 in Figure 2 allow the direct correlation of the initial increase in anodic current (denoted as P1 in Figure 1) to the reduction peak P′1 in the reverse scan. Restricting the anodic potential limit to $+165$ mV reproduces the CV curve which was published previously [21]. Shifting the potential limit only 12 mV further in the anodic direction (CV 3 in Figure 2) causes the appearance of P2 in the positive scan and the occurrence of P′2 in the reverse scan. Not only does the peak maximum of P′2 increase when the anodic potential limit is set to higher potentials but the position of P′2 gradually shifts towards lower potentials. The maximum of P2 at $+212$ mV, by contrast, is unaffected by the change in the anodic potential limit. P′3, located between P′1 and P′2 on the potential scale, emerges only when the anodic potential limit is set above $+250$ mV (CV 4 in Figure 2). An exponential increase in the dissolution current is observed only at potentials higher than $+360$ mV (marked by the black arrow in CV 7 in Figure 2). Corresponding to this dissolution a further cathodic

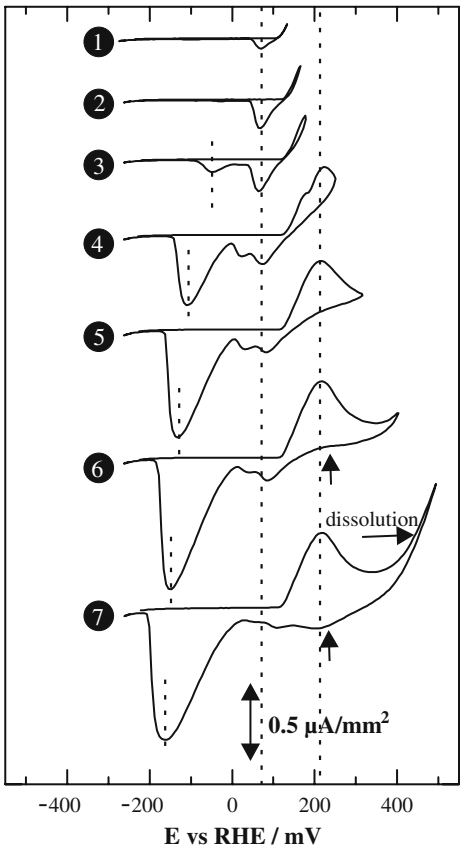

Fig. 2. Compound formation during copper dissolution: Gradual emergence of anodic and cathodic peaks upon shifting the potential limit, $dE/dt = 10$ mV s^{-1}.

"bump" emerges in the reverse scan that can be attributed to the re-deposition of copper material (small arrows in CV 6 and 7 in Figure 2). Comparing Figures 1 and 2 it is evident that the onset potential of anodic copper dissolution is shifted more than 70 mV to higher potentials when iodide is present. Similar behavior to that described in Figure 2 has been reported by Inukai et al. [23] for a Cu(111) surface exposed to an iodide containing perchloric acid. The additional current features were explained in terms of CuI film formation, thus passivating the electrode against dissolution. The same explanation as given by Inukai et al. [23] is assumed for the Cu(100) electrode in the iodide containing sulfuric acid. The supporting electrolyte (perchloric or sulfuric acid) is not believed to play a key role for this binary compound formation.

3.2. *Atomic structure and surface morphology*

The quality of the copper surface was routinely checked in the pure supporting electrolyte (0.5 mM H_2SO_4). STM images of Cu(100) in dilute sulfuric acid solution (Figure 3) reveal the characteristic surface morphology in the absence of condensed and ordered anion layers. Mono-atomically high substrate steps appear frayed due to a high kink density at step edges combined with a high diffusivity of copper atoms along these steps. On

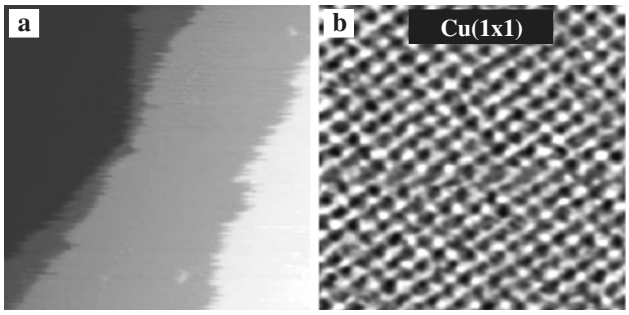

Fig. 3. Surface morphology and atomic structure of Cu(100) exposed to the pure supporting electrolyte (5 mM H_2SO_4), (a) 43 × 43 nm, $I_t = 5$ nA, $U_{bias} = 35$ mV, $E_{work} = +100$ mV; (b) 3.8 × 3.8 nm, $I_t = 5$ nA, $U_{bias} = 35$ mV, $E_{work} = +90$ mV.

the atomic scale only the bare (1 × 1) structure is observed (Figure 3b) within the entire double layer regime [13, 16].

An electrolyte exchange procedure as described in the experimental section instantaneously leads to the formation of a laterally ordered iodide adlayer (Figure 4). Iodide anions form a distorted "pseudo"-square structure on Cu(100) [21, 24] which is commensurate in only one of the substrate ⟨011⟩ directions resulting in an additional one-dimensional height modulation (Figure 4(a–b)). This structure can be described by a distorted c(2 × 2) unit cell which is expanded parallel to only one of the original unit-cell vectors. In the following we denote this regular iodide adsorbate structure as phase I. The *p*-vector decreases (increases) with increasing (decreasing) potentials in terms of a so called electrocompression (electrodecompression) process. Figure 4(c) presents a schematic hard-sphere model comparing the original c(2 × 2) and the derivative c(p × 2) unit-cell. The iodide saturation coverage of $\theta = 0.4$ ML is reached at +80 mV. The corresponding *p*-value amounts to $p = 2.5$ with a Nearest Neighbor Distance (NND) of 0.409 nm. A more refined structure model of the iodide saturation layer based on *in situ* X-ray diffraction experiments also reflects slight local distortions within the c(p × 2) layer. This topic will be addressed in a forthcoming paper [25].

Sweeping the electrode potential from +80 mV to +100 mV initiates a *local* dissolution of copper material (Figure 5(a–b)) in the presence of the c(p × 2)-I layer. This process preferentially starts at step edges and proceeds via an "inverse step-flow" mechanism (white arrows in Figure 5(b). Although the covering iodide layer is not in full registry with the underlying copper lattice, steps stabilize themselves during dissolution along preferential directions which coincide with main symmetry axes of the iodide lattice [21]. Most stable copper steps are not aligned parallel to the "commensurate" direction of the iodide adlayer but parallel to the densely packed iodide rows (see dashed lines in Figure 5a). Crossing step edges enclose angles which slightly deviate from 90° according to the reduced symmetry of the c(p × 2) lattice with respect to the

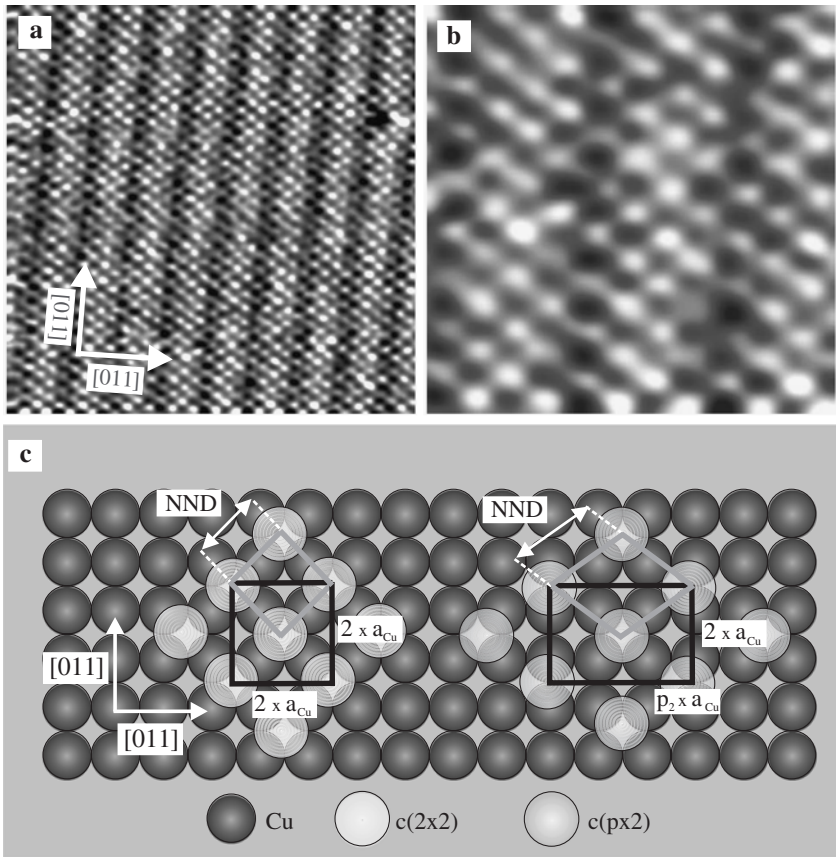

Fig. 4. Structure of the c(p × 2)-I layer at the onset of dissolution, (a) 15.1 × 15.1 nm, I_t = 5 nA, U_{bias} = 1 mV, E_{work} = +80 mV; (b) 4.7 × 4.7 nm, I_t = 5 nA, U_{bias} = 1 mV, E_{work} = +80 mV; (c) Structure model of the "original" c(2 × 2) and the derivative c(p × 2) adlayer, the *p*-value amounts to $p = 2.5$ at E_{work} = +80 mV.

Cu(100) substrate. Besides the local removal of copper material from step edges one observes the growth of an ordered film in close proximity to the dissolving terraces (Figure 5(b)). It is evident that both processes are correlated with each other.

The lateral structure on-top of this growing film (denoted in the following as phase II) significantly differs from the c(p × 2)-I adsorbate phase. Clearly visible is a striped long-range superstructure with a height modulation of 0.05 ± 0.01 nm and a periodicity of about 4.45 ± 0.05 nm (Figure 5(d)) perpendicular to these stripes. At these larger image sizes (Figure 5(a–b)) the significantly smaller long-range height modulation of the c(p × 2)-I layer cannot be seen.

The growth of a completely new phase is concluded from one-dimensional cross sections over the growing film in the sub-monolayer regime (Figure 5(c–d)). Measured step heights of 0.38 ± 0.01 nm (Figure 5(d)) do not correspond to mono-atomic steps on Cu(100) (Cu–Cu step: 0.18 nm). Height differences of 0.18 nm between two adjacent terraces both covered with phase II again indicate single Cu–Cu steps (Figure 5(d)). Characteristically, the 2D film growth starts within a narrow potential range of only 10 mV between +100 mV and +110 mV at the on-set of the anodic peak system P1/P2/P3 and proceeds until the entire electrode surface is covered. One reasonable explanation for these observations is the formation of an ultra-thin 2D-CuI film. Since STM does not provide a chemical sensitivity our assignment to 2D-CuI is based on a comparison to the work by Andryushechkin et al. [26, 27]. In fact, these authors observed with STM and LEED the same sequence of iodine/iodide phases on Cu(100) as a function of iodine exposure in UHV [26, 27] as we have seen by *in-situ* STM under electrochemical conditions as a function of the applied potential [21, 22, 24]. Beyond this similarity in the regular adsorbate phases there is even a striking correspondence between the atomic structure of our supposed 2D-CuI film (Figures 5–8) and that grown under UHV conditions. This latter UHV-grown film could, indeed, be identified as CuI using Auger electron spectroscopy [27].

Figure 6 provides a first impression on the atomic-scale structure of the initial 2D-CuI film (phase II). However, an ongoing altering of the film structure significantly hampers the imaging quality. Characteristically, phase II cannot be stabilized at any potential and has to be considered as a transient phase that evolves only when the film growth is fast. Superimposed to the striped long-range height modulation is a pseudo-hexagonal structure (see also white dots in Figure 6(c)) with an NND of 0.42 ± 0.02 nm. Only within a quite narrow potential window between +110 and +120 mV the 2D-CuI film can be stabilized. Above +120 mV the dissolution reaction sets in again, but now in the presence of the 2D-CuI film.

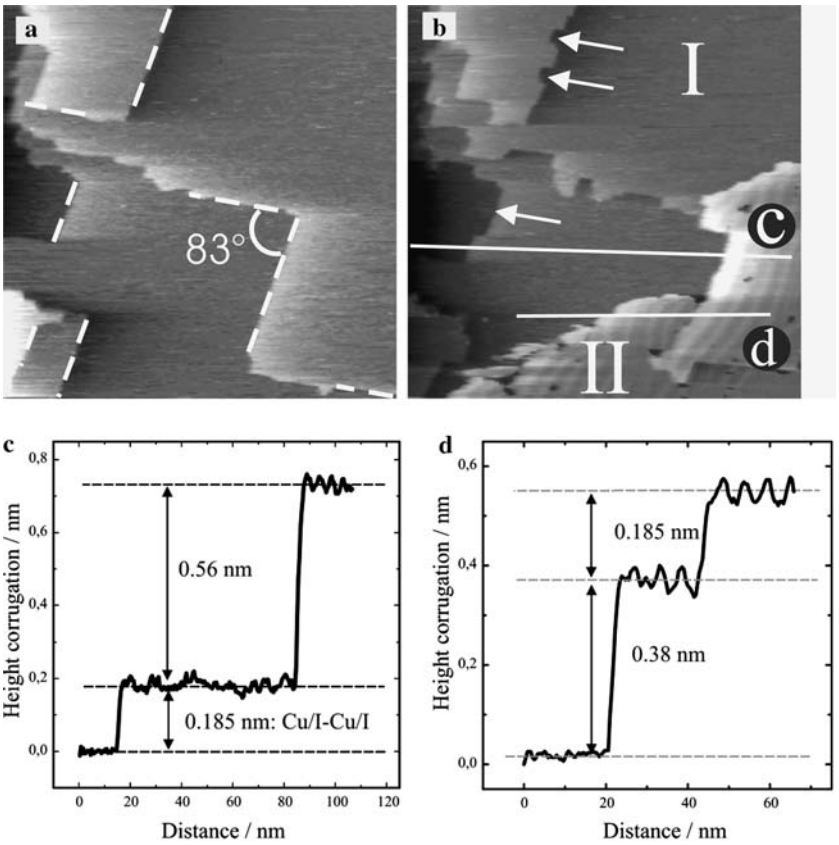

Fig. 5. Simultaneously occurring dissolution and growth of the 2D-CuI (phase II type), (a) 108 × 108 nm, I_t = 0.25 nA, U_{bias} = 224 mV, E_{work} = +110 mV; (b) 108 × 108 nm, I_t = 0.25 nA, U_{bias} = 224 mV, E_{work} = +110 mV; (c–d) Cross sections along the white lines in (b). (Please note: both STM images presented in Figure 5 are slightly filtered. The cross-sections, however, are taken from the original unfiltered images).

While Figure 7(a) represents the copper surface covered by the c(p × 2)-I layer (phase I) the 2D-CuI film (phase II) is already present in the following STM picture. All STM images indicate that step edges recede in the presence of the 2D-CuI film according to an ''inverse step flow mechanism''. Ongoing surface dynamics do not solely affect steps but also the structure of the initial 2D-CuI film on terraces. With time, the long-range height modulation of the initial 2D-CuI film (phase II) disappears in line with the appearance of a new 2D-CuI phase (denoted in the following as phase III). Step heights remain unaltered upon transition of phase II into phase III (Figure 7(f)). This new 2D-CuI phase evolves not only at terraces by conversion of the pre-existing phase II into phase III but also appears at lower terraces when step edges recede upon dissolution (e.g. see black arrows in Figure 7(c–d)). Terraces covered by the transient phase II are much more affected by the dissolution than terraces covered by the energetically more stable phase III. Both 2D-CuI films contain a certain concentration of local point defects (Figures 7 and 10) right after the film growth. These defects are imaged as little dark holes in the film. Their concentration decreases with time.

Similar to phase II also phase III reveals a striped pattern but with a significant smaller height corrugation of only 0.02 nm (Figure 8(d)). While the stripes of phase II exhibit a strong tendency to meandering (Figure 7) stripes of phase III are arranged in a strictly parallel manner revealing two distinct periodicities of $d1 = 1.7 \pm 0.2$ nm and $d2 = 3 \pm 0.2$ nm (Figure 8(a)) with no apparent regularity in the sequence of these characteristic stripe distances. Figures 8b,c show an almost ideal hexagonal symmetry of the CuI phase with an NND of 0.44 ± 0.02 nm. Local deviations from that value are due to the existence of periodically arranged dislocations. Atomic rows in adjacent stripes exhibit a pronounced anti-phase behavior as indicated by the dashed lines in Figure 8c. The enclosing angle between the stripe propagation direction and close packed rows on the atomic scale amounts to $8 \pm 2°$ (Figure 8(b)). Densely packed rows of the 2D-CuI film enclose an angle of $44 \pm 2°$ with one of the substrate ⟨110⟩ directions (dashed line in Figure 8(b)) Andryushechkin et al. [27] already pointed out that the main difference between phase II and III consists in their relative orientation with respect to the copper substrate while their interatomic spacings and their symmetry properties are very similar.

Three reactions of the 2D-CuI film (phase III type) are in the following of particular interest:

(a) the decay of the 2D-CuI (phase III type) in the reverse potential scan
(b) the anodic copper dissolution in the presence of the 2D-CuI film (phase III type) and
(c) the growth of 3D-CuI at higher dissolution rates.

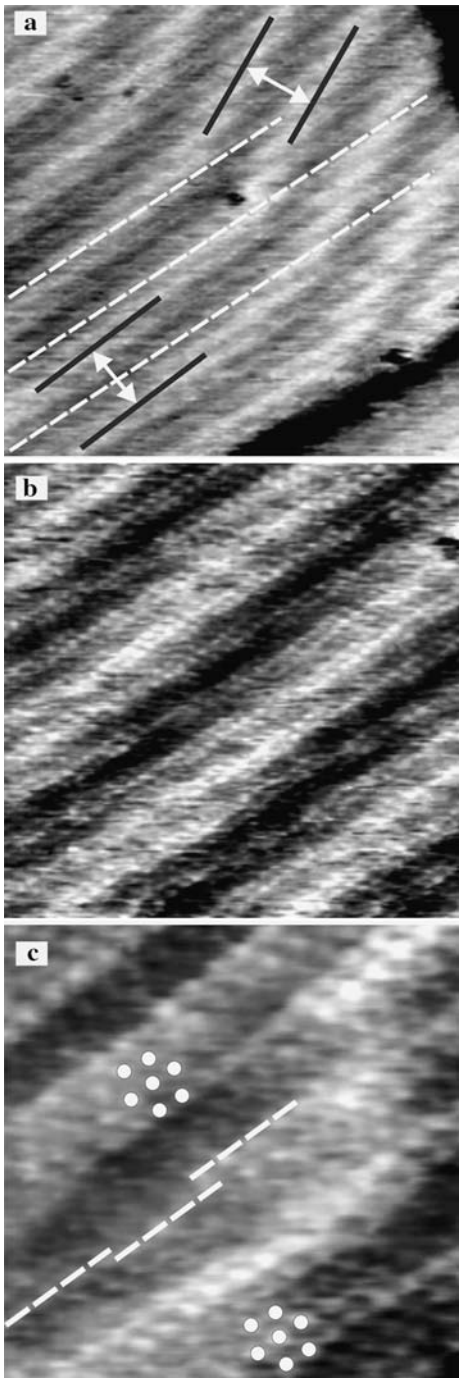

Fig. 6. Atomic structure of the initial 2D-CuI film (phase II type), (a) 25 × 25 nm, I_t = 0.1 nA, U_{bias} = 89 mV, E_{work} = +120 mV; (b) 13 × 13 nm, I_t = 0.25 nA, U_{bias} = 224 mV, E_{work} = +120 mV; (c) 6.3 × 6.3 nm, I_t = 0.25 nA, U_{bias} = 224 mV, E_{work} = +120 mV.

Changing the potential from +110 mV back to +90 mV initiates the decay of the 2D-CuI phase (Figure 9). Apparently, the potential dependent appearance and disappearance of the 2D-CuI film can be regarded as reversible with a small potential hysteresis of about 20 mV. Active sites in the dissolving process are domain boundaries, point defects or regular step edges of the 2D-CuI film. Figure 9(a) represents the surface just after the initial break-up of the 2D-CuI film. As a function of time and potential the 2D-CuI phase shrinks until the film has completely disappeared from the surface. It should be noted that the decay of the 2D-CuI film does not proceed via the intermediate phase II indicating that the previous transition from phase II to III was irreversible.

Copper steps aligned parallel to directions similar to those in Figure 5(a) become visible immediately after break-up of the 2D-CuI film. Such a step alignment can be seen as a clear hint for the presence of the c(p × 2)-I lattice in this "submonolayer" regime of the dissolving 2D-CuI film. However, the atomic scale imaging of the c(p × 2)-I lattice is somewhat impeded by the presence of a disordered layer, probably remnants of the dissolving 2D-CuI film which diffuse on-top of the c(p × 2)-I adlayer. Only when drastic tunneling conditions were applied these remnants are swept away by the tunneling tip, thus allowing to image the c(p × 2)-I (not shown here). These remnants completely disappear when the potential is set below +50 mV.

When the potential is swept in the anodic direction in the presence of an intact and stable 2D-CuI film (phase III type) the copper dissolution is again initiated. Time resolved STM images clearly indicate an inverse step flow mechanism (Figure 10). Step edges recede leaving the same 2D-CuI film at the corresponding lower terraces behind.

The dissolution process becomes, however, hampered when the potential is set above +125 mV. At these slightly higher potentials the dissolution is accompanied by the appearance of 3D-CuI clusters. This process preferentially starts at step edges and proceeds until the entire surface is covered with 3D-CuI. Under these conditions surface imaging becomes more and more difficult due to the reduced conductivity of CuI_{bulk} (denoted as phase IV in the following). Figure 11 displays a successful STM image showing a "cloudy" cluster structure at the surface. Only a few flat areas (marked by white arrows in Figure 11(a)) remain uncovered. Cluster heights up to 8.6 nm can be detected in one-dimensional cross-sections (Figure 11(b)). In order to get rid of these 3D-CuI clusters the reduction peak P′2 has to be passed. This indicates a considerably larger hysteresis for the *appearance* and *disappearance* of the CuI_{bulk}compared to the 2D-CuI phases. The peak-to-peak separation between P2/3 and P′2 in Figure 1 amounts to ΔE = 320 mV.

4. Discussion

The huge differences in the cyclic voltammograms of copper electrodes in iodide containing electrolytes (Figures 1 and 2) and in other acidic electrolytes [11–17] are due to the intermediate and final products formed upon copper dissolution.

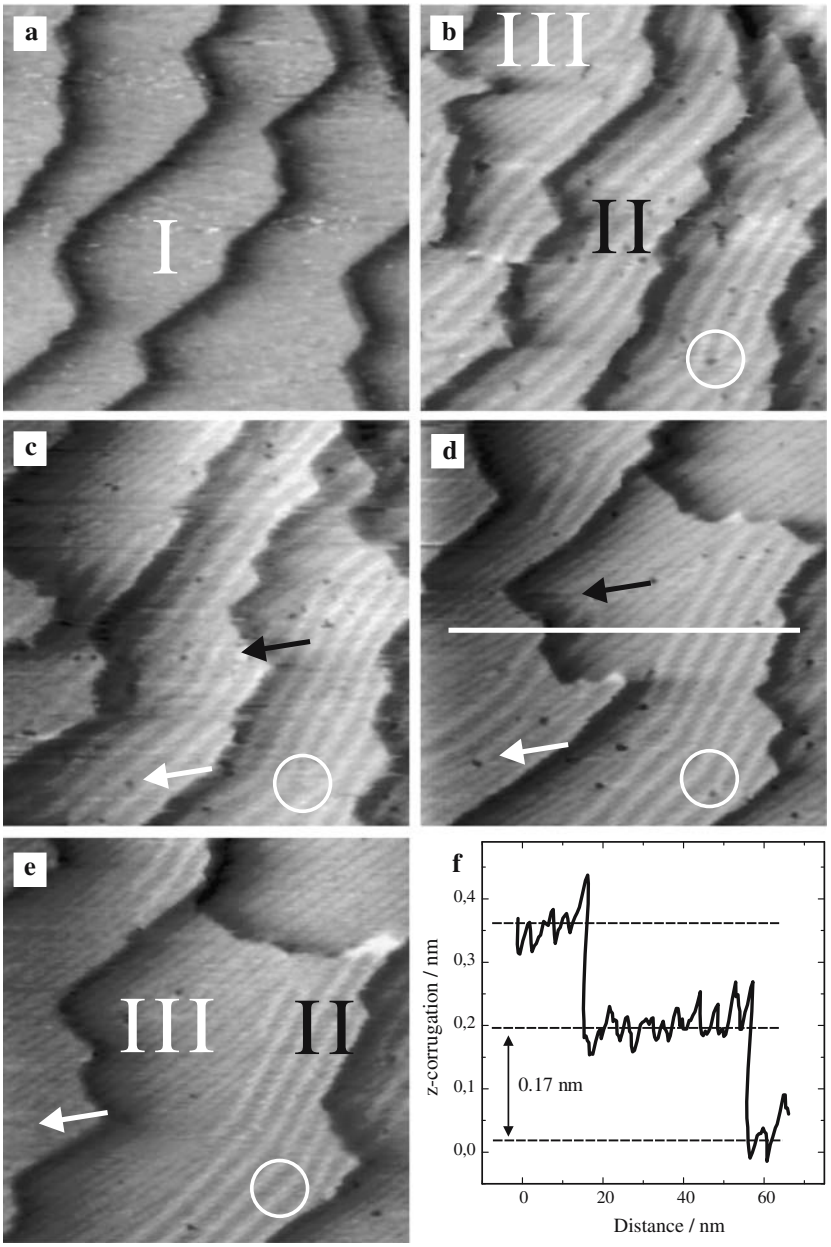

Fig. 7. Coexistence of the transient (phase II type) and the stable (phase III) 2D-CuI film, (a–e) 108 × 108 nm, I_t = 0.1 nA, U_{bias} = 101 mV, E_{work} = +120 mV; (f) One-dimensional cross-section along the white line in (d).

In the absence of complexing anions copper dissolution is described by the widely accepted Bockris–Mattson mechanism [28–30]. According to that, copper electro-oxidation occurs via two single electron transfer processes with the transition of cuprous Cu^+ to cupric Cu^{2+} ions as the rate determining step. Final dissolution products in sulfuric acid electrolytes are octahedral $[Cu(H_2O)_6]^{2+}$ aquo-complexes. Their high solubility explains the absence of additional current features in the CVs despite the exponential increase of the anodic dissolution current followed by the corresponding re-deposition peak in the reverse scan.

In the presence of complexing anions, e.g. in hydrochloric acid [13], cuprous Cu^+ species are formed probably as intermediate CuCl monomers. It is well known that strongly complexing anions stabilize cuprous ions even in aqueous solutions so that Cu^+ species are not necessarily further oxidized to cupric Cu^{2+} species. Instead, highly soluble $[CuCl_2]^-$ chloro-complexes are formed and subsequently transported in solution [31, 32].

Copper electro-oxidation in the presence of iodide also starts with the formation of *cuprous* Cu^+ species. On the basis of electrochemical and SERS experiments $[CuI_2]^-$ iodo-complexes are discussed as intermediate species in the course of the copper dissolution [33]. However, these cuprous iodide complexes are energetically not stable in aqueous solutions.

It is the low solubility product of CuI_{bulk} with $K_s = 1.2 \times 10^{-11.3}$ mol^2 l^{-2} [34] that governs copper dissolution in the presence of iodide anions. Highly insoluble CuI phases are formed upon copper dissolution:

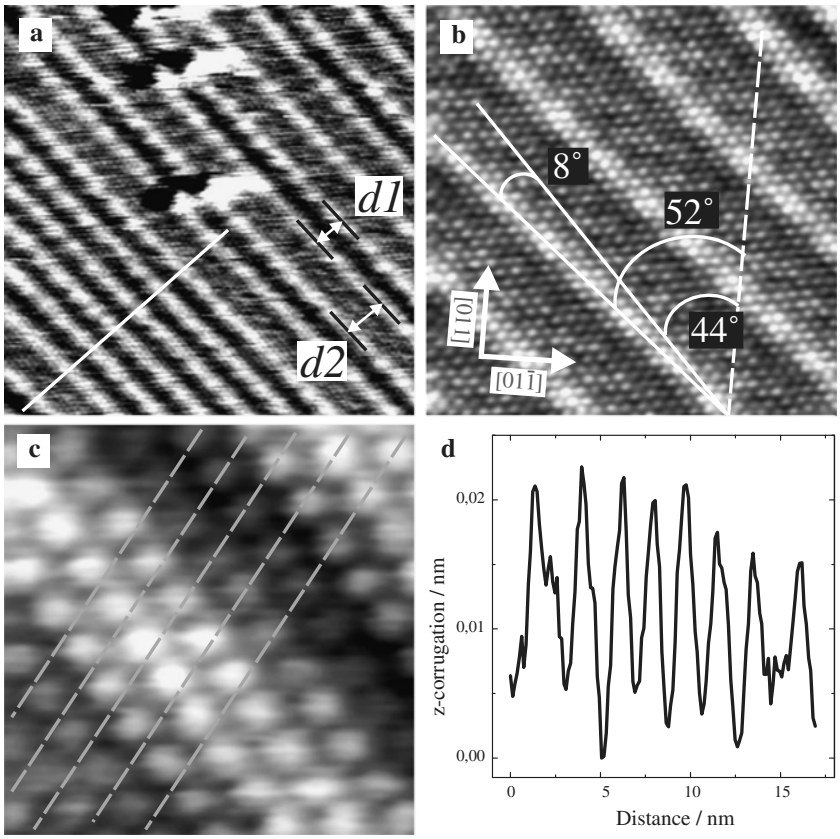

Fig. 8. Atomic structure of the stable 2D-CuI film (phase III type), (a) 27.3 × 27.3 nm, I_t = 1.3 nA, U_{bias} = 10 mV, E_{work} = +120 mV; (b) 12.1 × 12.1 nm, I_t = 1.3 nA, U_{bias} = 10 mV, E_{work} = +120 mV; (c) 3 × 3 nm, I_t = 1.3 nA, U_{bias} = 10 mV, E_{work} = +120 mV; (d) Cross-section along the white line in (a).

$$Cu \rightarrow Cu^{+} + e^{-} \quad \text{(electro-oxidation)} \tag{1}$$

$$Cu^{+} + I^{-} \rightarrow CuI \quad \text{(complexing)} \tag{2}$$

$$n\text{CuI} \rightarrow (\text{CuI})_n \quad \text{(phase formation of solid CuI)} \tag{3}$$

As a consequence a thick passivating CuI film can kinetically hinder further copper dissolution. Only when significantly higher potentials are applied does the passive film break up, giving rise to the restart of the dissolution process (CV 7 in Figure 2). At these extremely high overpotentials copper dissolution probably proceeds via a direct two-electron transfer [31, 32] to cupric Cu^{2+} ions (4). However, these cupric species are thermodynamically not stable in solution if iodide anions are also present [34]. *The electro-oxidized cupric* Cu^{2+} ions are *chemically* reduced to *cuprous* Cu^{+} ions with iodide acting as reductive reagent (5). As a consequence, insoluble 3D-CuI clusters as the final product of this reaction precipitate at the electrode surface. Molecular iodide formed as a side product at these potentials (5) should be directly electro-reduced at the surface to iodide anions (6):

$$Cu \rightarrow Cu^{2+} + 2e^{-} \quad \text{(electro-oxidation)} \tag{4}$$

$$2Cu^{2+} + 4I^{-} \rightarrow 2CuI + I_2 \quad \text{(chemical reduction)} \tag{5}$$

$$I_2 + 2e^{-} \rightarrow 2I^{-} \quad \text{(electro-reduction)} \tag{6}$$

However, due to the electrode passivation the iodine reduction (6) might be kinetically hindered thus leading to a co-precipitation of molecular iodine and 3D-CuI clusters onto the electrode surface under these extreme conditions.

The apparent complexity of the CV (Figures 1 and 2) can be explained by the appearance and disappearance of various CuI phases differing in their structural relation to the copper substrate. Besides the 2D-CuI film which exhibits a well defined epitaxial relation to the substrate 3D-CuI clusters emerge above +120 mV at step edges via nucleation and growth (Figure 11) at the surface. At even higher potentials 3D-CuI clusters are formed most likely by a dissolution/precipitation mechanism. Precipitated CuI clusters with a "loose" relation to the electrode surface reveal a significantly larger potential hysteresis concerning their appearance and disappearance than those CuI phases which are in direct contact to the electrode.

All previous STM related studies on copper dissolution in chloride or bromide containing electrolytes did not report the formation of copper halides. This can simply be attributed to the higher solubility product of $CuBr_{bulk}$ ($K_s = 5.9 \times 10^{-9}$ mol^2 l^{-2} and $CuCl_{bulk}$ ($K_s = 1.72 \times 10^{-7}$ mol^2 l^{-2} and the low halide concentrations of 10 mM used in previous experiments [11–13, 17].

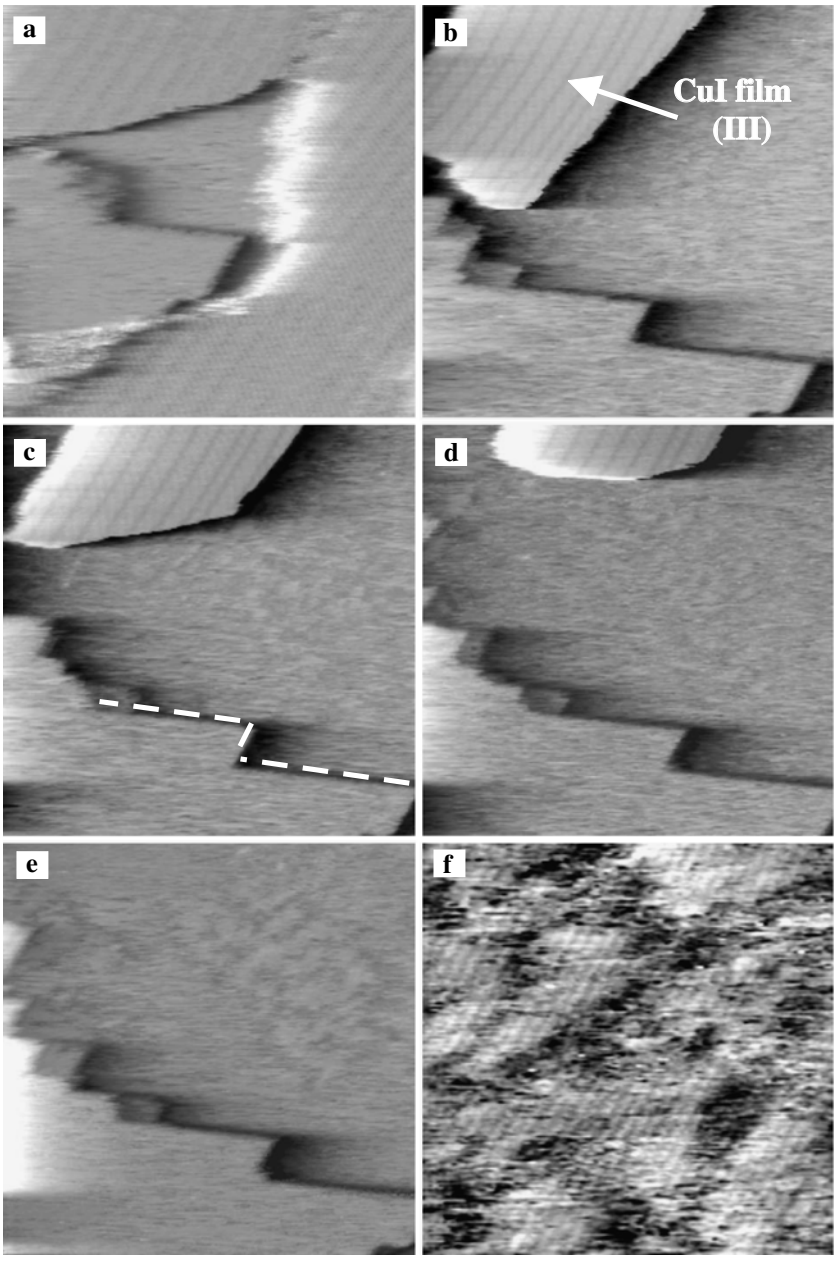

Fig. 9. Decay of the 2D-CuI film (phase III) in the reverse potential scan, (a) Surface morphology after break-up of the 2D-CuI film, 67 × 67 nm, I_t = 1 nA, U_{bias} = 35 mV, E_{work} = +105 mV; (b–e) 81 × 81 nm, I_t = 3.7 nA, U_{bias} = 104 mV, E_{work} = +105 mV; (f) Disordered phase on-top of the c(p × 2)-I adlayer, 20.4 × 20.4 nm, I_t = 0.1 nA, U_{bias} = 248 mV, E_{work} = +90 mV.

It can be assumed that CuX_{bulk} phases (X = Br^-, Cl^-) would also appear upon copper dissolution provided higher chloride and bromide concentrations are used. E.g., Dobelhofer et al. report the formation of crystalline $CuCl_{bulk}$ and $CuBr_{bulk}$ upon copper deposition from acidic electrolytes containing 0.3 M $CuSO_4$, 2.2 M H_2SO_4 and trace amounts of halides (2 mM Br^- or Cl^-, respectively) [35]. Here, it is the high concentration of cuprous ions which gives rise to the exceeding of the CuX_{bulk} solubility product upon copper deposition.

For the potential regime where the 2D-CuI film on Cu(100) is formed we assume a similar scenario as previously discussed for a chloride covered Cu(111) surface [36–38]. Depending on the applied potential a stationary equilibrium concentration of diffusing copper halide species on-top of the anion covered electrode surface is established with substrate steps acting as "*sources*" for a gaseous like phase of mobile CuI species on terraces. A potential increase lets the concentration of mobile CuI monomers on terraces increase until a critical threshold is exceeded. This threshold can be regarded as the 2D analogon to the solubility product (K_s). In the present case, the solubility product is locally exceeded at the surface which explains the surface confined formation of CuI.

Recently we succeeded in visualizing the initial stage of 2D-CuI nucleation on terraces of a Cu(111) surface as expected from the scenario described above [25].

Due to the consumption of mobile CuI monomers by the growth of 2D-CuI islands the equilibrium between

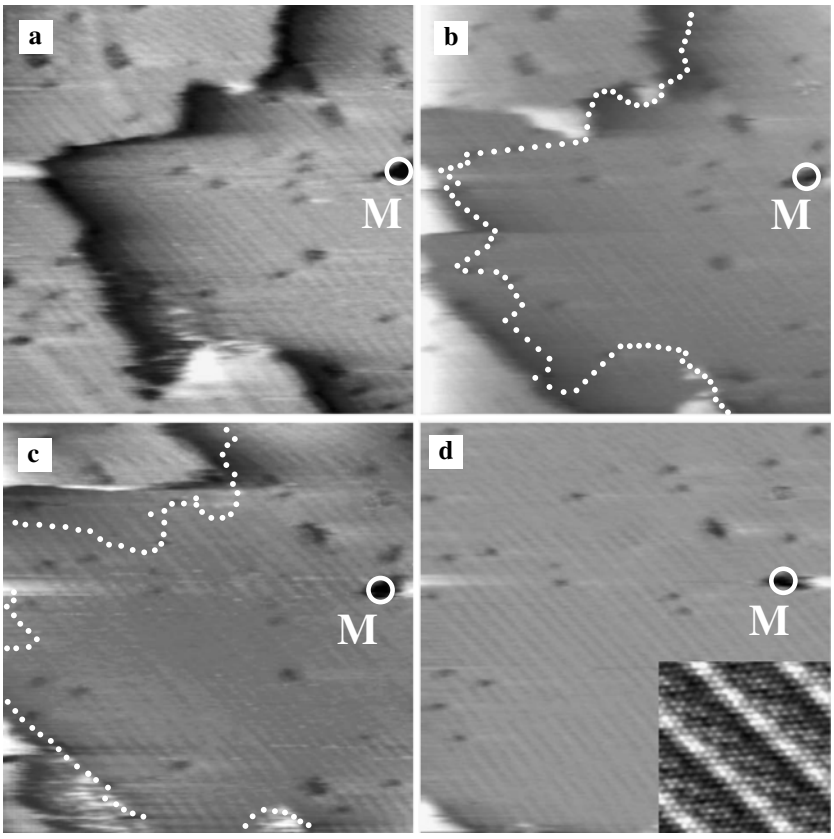

Fig. 10 Dissolution in the presence of the 2D-CuI film (phase III type), (a–d) 70 × 70 nm, I_t = 1 nA, U_{bias} = 5 mV, E_{work} = +120 mV. In order to facilitate the recognition of this inverse step flow the exact course of step edges in the precedent STM image is marked in the STM images. One prominent defect within the 2D-CuI film is marked. The in-set in panel (d) shows the atomic structure of the 2D-CuI film on terraces which are affected by the ongoing dissolution.

substrate steps and mobile CuI species on terraces is disturbed. The growing 2D-CuI islands act as "sinks" for mobile CuI species. Hence, it is not the massive copper dissolution which causes the nucleation and growth of CuI at the surface. The further growth of 2D-CuI islands involving consumption of copper material provokes the accelerated etching of step edges resulting in a net flux of copper material from copper steps to step edges of the growing 2D-CuI film (Figure 5(b)).

However, the 2D-CuI film growth cannot be regarded as a simple "surface confined precipitation" of CuI under pure kinetic control. In fact, the initial 2D growth resulting in a kind of CuI "wetting layer" with a well defined structural relation to the underlying substrate and the transition of the 2D into a 3D growth mode in an advanced stage of CuI formation is clearly pointing to a kind of "Stranski–Krastanov"-like behavior similar to the growth mode of CuI on Cu(100) under UHV conditions [27].

Provided potentials between +100 mV and +120 mV are applied the 2D-CuI film exhibits a high structural stability and remains stable even for several hours. Since the 2D-CuI "wetting layer" appears at potentials below the regime of the 3D-CuI growth we denote the observed effect as Under Potential Formation (UPF) of a binary compound similar to the well known phenomenon of Under Potential Deposition (UPD) of metallic films [39], 2D-compound layers [40, 41] or binary ionic layers [42]. In these latter cases all "deposit" components come from the solution phase while in the present case the metal ions originate directly from the electrode surface as a consequence of an oxidative dissolution reaction of the electrode material.

While *Under Potential Deposition (UPD)* is a pure thermodynamic phenomenon *Under Potential Formation (UPF)* of a binary compound is the result of the complex interplay between dissolution and growth kinetics and the interface thermodynamics.

A preliminary structure model (Figure 12) of the 2D-CuI film is based on the following stacking sequence of atomic layers: Cu(100)/I(adsorbed)/Cu^+/I. This is in agreement with previous results by Andryushechkin et al. [27]. These authors suggested a 2D-CuI film on Cu(100) that exhibits a close structural similarity to a (111) lattice of CuI_{bulk}. This binary compound crystallizes in an fcc ZnS-type (zinc blende) structure with tetrahedral coordination of iodide and copper, respectively [34]. Due to the reduced symmetry of the c(p × 2)-I adsorbate phase with respect to the underlying substrate there are also somewhat distorted "quasi"-threefold hollow sites available within the iodide adsorbate layer as potential adsorption sites for cuprous ions (Figure 4(c)). With an additional iodide particle on-top of this single Cu^+ ion it is possible to form a slightly distorted tetrahedron with a central monovalent Cu species surrounded by 4 iodide particles as a character-

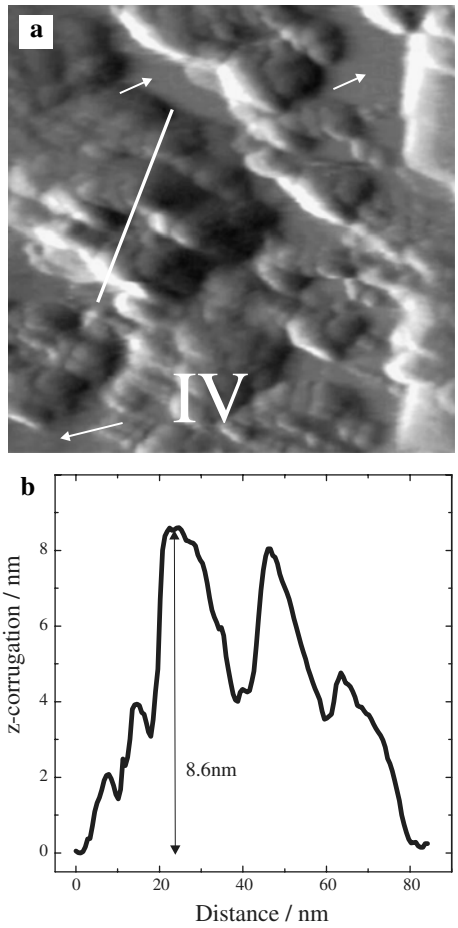

Fig. 11. Appearance of 3D-CuI clusters upon copper dissolution, (a) 142 × 142 nm, I_t = 1.7 nA, U_{bias} = 93 mV, E_{work} = +110 mV; (b) One-dimensional cross-section along the white line in (a).

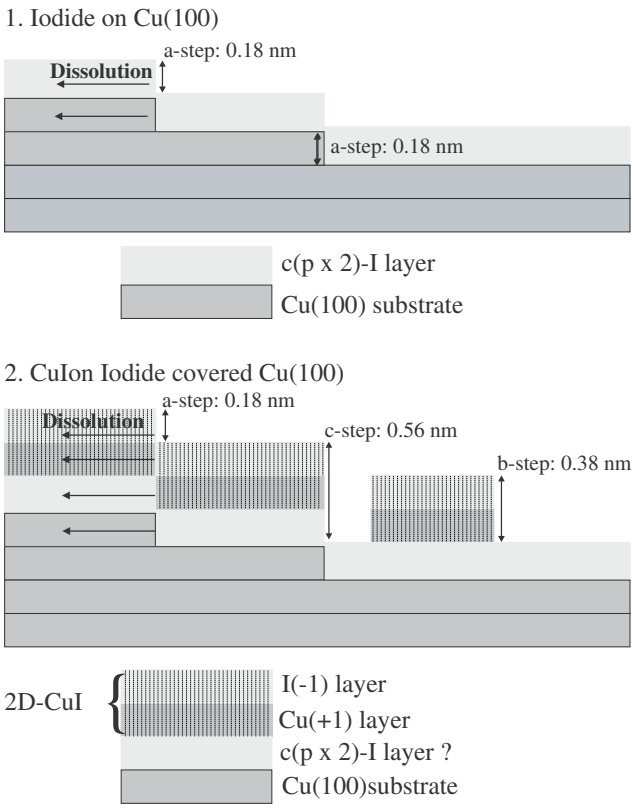

Fig. 12. Schematic drawing illustrating the vertical stacking sequence of the Cu(100)/I and Cu(100)/I(adsorbate)/Cu^+/I systems.

istic structure motif of the growing 2D-CuI film. Bright "dots" in the atomically resolved STM images can thus be assigned to the terminating iodide species. The proposed stacking sequence of atomic layers in the 2D-CuI film is also in agreement with the observed step heights in the 2D-CuI submonolayer regime (Figure 7). The apparent step height of 0.38 nm under the given tunneling conditions (Figure 5(c)) does not correspond to a single copper step but points to a thicker film, most likely composed by one monolayer of cuprous ions and the terminating iodide layer (b-step in Figure 12). From the crystalline 3D-CuI phase one would expect an interlayer spacing of 0.35 nm between neighbored iodide layers parallel to the (111) plane. One reasonable explanation for the observed slight differences in expected and measured step heights could be related to the fact that STM images do not simply reflect the pure surface topography but also the surface electronic properties in terms of a local density of state. An increased step height in the STM experiment could originate from a decreased conductivity in the presence of the 2D-CuI film. Due to the different lattice symmetries and the slight mismatch between nearest neighbor spacings in the c(p × 2)-I phase (NND_{iodide} = 0.41 nm) and an ideal CuI(111) plane (NND_{iodide} = NND_{Cu} = 0.428 nm), these lattices are apparently not in full registry. The appearance of striped dislocation lines (Figure 8) in combination with the pronounced anti-phase behavior could be explained in terms of a partial release of lateral stress which originates from the inherent lattice mismatch. An ultimate structure model including the "buried" interface between the copper substrate and the first iodide layer, however, cannot be achieved only on the basis of the present STM work. In particular the assumption by Andryushechkin et al. [27] of an intact c(p × 2)-I layer in the presence of the 2D-CuI layer [27] has to be verified by more sophisticated experiments such as *in-situ* X-ray diffraction.

As demonstrated in Figure 10 the 2D-CuI film does not efficiently passivate the electrode surface against further dissolution. An ongoing dissolution in the presence of the 2D-CuI film is also characterized by an "inverse" step flow mechanism. Considering the proposed stacking sequence at the interface (Figure 12) it becomes obvious that the dissolution mechanism in the presence of the 2D-CuI film must be much more complex than for electrode surfaces which are covered by monolayers of regular adsorbate phases [11–17]. In this latter case only two layers are involved in the dissolution process, namely the anion overlayer and the topmost substrate layer, while in the present case 4 layers must participate in the "collective receding" of steps (Figure 12).

Copper material dissolved by this inverse step flow does not leave the surface but is consumed by the

nucleation and subsequent growth of 3D-CuI clusters. At least in the initial stage of cluster formation the copper material comes from these step edges.

It is the approximately 8 nm thick CuI film (phase IV) which acts as a passivation layer against copper dissolution. Even thicker CuI films may occur at higher potentials (above +350 mV) via dissolution and subsequent precipitation from the solution phase.

5. Conclusions

A laterally well ordered 2D-CuI film is formed on Cu(100) at potentials (+100 mV–+110 mV) below the potential range of the corresponding CuI_{bulk} formation (above +120 mV). The observed structural features of the 2D-CuI film are in good agreement with assumption of a Cu(100)/I(adsorbed)/Cu^+/I stacking sequence. Due to the pronounced hexagonal symmetry of the growing film we propose a lateral structure of the 2D-CuI film which is closely related to the (111)-plane of crystalline CuI_{bulk} (zinc blende type) with Cu^+ ions placed within a kind of "sandwich" of two adjacent iodide layers. Quite surprisingly, the formation of the 2D-CuI film does not efficiently suppress the copper dissolution. An inverse step flow mechanism is also observed in the presence of the 2D-CuI film above +120 mV. Higher reaction rates lead to the growth of 3D-CuI clusters thus explaining the final passivation against dissolution as observed in the CV.

References

1. P.C. Andriacos, C. Uzoh, J.O. Ducovic, J. Horcans and H. Deligianni, *IBM J. Res. Dev.* **42** (1998) 567.
2. L. Arnaud, G. Tartavel, T. Berger, D. Mariolle, Y. Gobil and I. Touet, *Microelectron. Reliab.* **40** (2000) 1295.
3. M.R. Vogt, W. Polewska, O.M. Magnussen and R.J. Behm, *J. Electrochem. Soc.* **144** (1997) L113.
4. W. Polewska, M.R. Vogt, O.M. Magnussen and R.J. Behm, *J. Phys. Chem. B* **103** (1999) 10440.
5. J. Scherer, M.R. Vogt, O.M. Magnussen and R.J. Behm, *Langmuir* **13**(26) (1997) 7045.
6. E. Szocs, G. Vastag, A. Shaban and E. Kalman, *Corr. Sci.* **47** (2005) 893.
7. N. Ikemiya, T. Kubo and S. Hara, *Surf. Sci.* **323** (1995) 81.
8. V. Maurice, H.-H. Strehblow and P. Marcus, *J. Electrochem. Soc.* **146** (1999) 524.
9. V. Maurice, H.-H. Strehblow and P. Marcus, *Surf. Sci.* **458** (2000) 185.
10. H.-H. Strehblow, V. Maurice and P. Marcus, *Electrochim. Acta* **46** (2001) 3755.
11. D.W. Suggs and A.J. Bard, *J. Am. Chem. Soc.* **116** (1994) 10725.
12. D.W. Suggs and A.J. Bard, *J. Phys. Chem.* **99** (1995) 8349.
13. M.R. Vogt, A. Lachenwitzer, O.M. Magnussen and R.J. Behm, *Surf. Sci.* **399** (1998) 49.
14. O.M. Magnussen and M.R. Vogt, *Phys. Rev. Lett.* **85** (2000) 357.
15. O.M. Magnussen, L. Zitzler, B. Gleich, M.R. Vogt and R.J. Behm, *Electrochim. Acta* **46** (2001) 3725.
16. O.M. Magnussen, *Chem. Rev.* **102** (2002) 679.
17. P. Broekmann, M. Anastasescu, A. Spaenig, W. Lisowski and K. Wandelt, *J. Electroanal. Chem.* **500** (2001) 241.
18. J. Kunze, V. Maurice, L.H. Klein, H.-H. Strehblow and P. Marcus, J. *Electroanal. Chem.* **554–555** (2003) 113.
19. J. Kunze, V. Maurice, L.H. Klein, H.-H. Strehblow and P. Marcus, *Corr. Sci.* **46** (2004) 245.
20. M. Wilms, M. Kruft, G. Bermes and K. Wandelt, *Rev. Sci. Instr.* **70**(7) (1999) 3641.
21. P. Broekmann, A. Spaenig, A. Hommes and K. Wandelt, *Surf. Sci.* **517**(1–3) (2002) 123.
22. P. Broekmann, A. Spaenig, A. Hommes and K. Wandelt (to be published).
23. J. Inukai, Y. Osawa and K. Itaya, *J. Phys. Chem. B.* **102** (1998) 10034.
24. A. Hommes, A. Spaenig, P. Broekmann and K. Wandelt, *Surf. Sci.* **547** (2003) 239.
25. P. Broekmann, S. Huemann, H. Zajonz, R. Hunger and K. Wandelt (to be published).
26. B.V. Andryushechkin, K.N. Eltsov, V.M. Shevlyuga, U. Bardi and B. Cortigiani, *Surf. Sci.* **497** (2002) 59.
27. B.V. Andryushechkin, K.N. Eltsov and V.M. Shevlyuga, *Surf. Sci.* **566–568** (2004) 203.
28. E. Mattson and J.O. Bockris, *Trans. Faraday. Soc.* **55** (1959) 1586.
29. U. Bertocci, *Electrochim. Acta* **11** (1966) 1261.
30. U. Bertocci and D.R. Turner. *in* A.J. Bard (ed.), Encyclopedia of Electrochemistry of the Elements III, (Marcel Dekker, New York, 1974), pp. 383.
31. D.Y. Wong, B.A.W. Coller and D.R. MacFarlane, *Electrochim. Acta* **38** (1993) 2121.
32. A. De Agostini, E. Schmidt and W.J. Lorenz, *Electrochim. Acta* **34** (1989) 1243.
33. D.E. Irish, L. Stolberg and D.W. Shoesmith, *Surf. Sci.* **158** (1985) 238.
34. Hollemann-Wiberg, Lehrbuch der Anorganischen Chemie, de-Gruyter (1995).
35. K. Dobelhofer, S. Wasle, D.M. Soares, K.G. Weil, G. Weinberg and G. Ertl, *Z. Phys. Chem.* **217** (2003) 479.
36. P. Broekmann, M. Wilms, M. Kruft, C. Stuhlmann and K. Wandelt, *J. Electroanal. Chem.* **467** (1999) 307.
37. M. Giesen and S. Baier, *J. Phys.: Cond. Matter.* **13** (2001) 5009.
38. M. Giesen, *Prog. Surf. Sci.* **68** (2001) 1.
39. S. Ye and K. Uosaki. *in* A.J. Bard and M. Stratmann (eds), Encyclopedia of Electrochemistry, Volume 1: Thermodynamics and Electrified Interfaces (Wiley-VCH, 2001).
40. B.W. Gregory and J.L. Stickney, *Electroanal. Chem.* **300** (1991) 543.
41. J.L. Stickney, T.L. Wade, B.H. Flowers, R. Vaidyanathan and U. Happek. *in* A.J. Bard and M. Stratmann (eds), Encyclopedia of Electrochemistry Volume 1: Thermodynamics and Electrified Interfaces. (Wiley-VCH, 2001).
42. R.R. Adzic and J.X. Wang, *J. Phys. Chem. B* **102** (1998) 6307.